34th Annual International Conference of the IEEE EMBS
San Diego, California USA, 28 August - 1 September, 2012

Determination of Neural State Classification Metrics from the Power Spectrum of Human ECoG*

Matthew Kelsey, David Politte, *Member, IEEE,* Ryan Verner, John M. Zempel, Tracy Nolan, Abbas Babajani-Feremi, Fred Prior, *Senior Member, IEEE* , and Linda J. Larson-Prior, *Member, IEEE*

Abstract— **Brain electrical activity exhibits scale-free dynamics that follow power law scaling. Previous works have shown that broadband spectral power exhibits state-dependent scaling with a log frequency exponent that systematically varies with neural state. However, the frequency ranges which best characterize biological state are not consistent across brain location or subject. An adaptive piecewise linear fitting solution was developed to extract features for classification of brain state. Performance was evaluated by comparison to an *a posteriori* based feature search method. This analysis, using the 1/*f* characteristics of the human ECoG signal, demonstrates utility in advancing the ability to perform automated brain state discrimination.**

I. Introduction

Automated discrimination of neural state has been a long standing goal [1-5]. Automatic state determination would prove useful in moving long-term monitoring from hospital to home settings. It would also enable novel methods for monitoring state in normal subjects in positions of high stress or sleep loss such as military personnel, shift workers or long-haul transport operators.

At present, defining changes in neural state is done based on human observation of changes in the electrical activity of the brain, accomplished using both time domain graphemes and/or changes in spectral content. To date, however, no automated method has proven robust to such subtle state changes as represented by rapid eye movement (REM) sleep, in which brain electrical signals are difficult to differentiate from the state of quiet wake [3, 6] .

Despite recent evidence that brain can exhibit local changes in state [7, 8], most detection methods rely on global measures to define distinct changes in neural state. Our work is based on the observation that the brain, like other complex dynamic systems, exhibits scale-free dynamics that follow power-law scaling [9-12] with a log-frequency exponent that varies globally between the states of awake and deep sleep (slow wave sleep, SWS) [13, 14].

Our previous work [15] introduced a best-fit Multivariate Maximum Likelihood Analysis (MMLA) technique to explore these scale-free properties of human ECoG. Our analysis provided new insight into characteristics of this property when the brain changes its state between awake and asleep. By allowing the data to define the regions over which linear slopes could be fit to log-log plots of signal power by frequency, we have shown that the ECoG spectrum is not well characterized by a single linear fit across a defined set of frequencies, but is best described by a set of discrete linear fits across the full range of frequencies available.

In this paper, we build upon our previous analyses to explore the use of the power law signatures of the global power spectral density (PSD) as state discriminatory features. We formalize the MMLA technique presented earlier and measure its efficacy in automatically determining piecewise linear fit endpoints, thereby modeling unlabeled data with scale-free slope line segments. The relative performance of this method is examined to assess its usefulness in optimally representing state-discriminatory characteristics of brain activity.

We develop an exhaustive search feature extraction benchmark against which to compare the value of the best-fit MMLA modeling approach. The benchmarking method is designed to search for sets of frequency ranges within which power law signatures support accurate classification of the source PSD and the brain state. The benchmark will establish useful limits of 1/*f* metrics independent of the best-fit method.

Based on the results of our analyes, we address the following questions:

1. Do power law signatures of ECoG PSDs contain discriminatory information between the stages of non-REM (NREM) sleep?
2. If so, is there a relationship between least-error piecewise linear signal representation and classifier performance?

*Manuscript received March 15, 2012. This work was supported in part by the McDonnell Foundation.

Matthew Kelsey is with the Mallinckrodt Institute of Radiology, Washington University School of Medicine, St. Louis, MO 63110 USA (e-mail: kelseym@mir.wustl.edu).

David Politte is with the Mallinckrodt Institute of Radiology, Washington University School of Medicine, St. Louis, MO 63110 USA (e-mail: politted@mir.wustl.edu).

Ryan Verner is with the Department of Biomedical Engineering, Washington University in St. Louis, St. Louis, MO 63110 USA (e-mail: vernerryan@wustl.edu).

John Zempel is with the Departments of Neurology and Pediatrics, Washington University School of Medicine, St. Louis, MO 63110 USA (e-mail: zempelj@neuro.wustl.edu).

Tracy Nolan is with the Mallinckrodt Institute of Radiology, Washington University School of Medicine, St. Louis, MO 63110 USA (e-mail: tracyn@npg.wustl.edu).

Abbas Babajani-Feremi is with the Department of Anatomy and Neurobiology, Washington University School of Medicine, St. Louis, MO 63110 USA (e-mail: abbasbf@pcg.wustl.edu).

Fred Prior is with the Mallinckrodt Institute of Radiology, Washington University School of Medicine, St. Louis, MO 63110 USA (e-mail: priorf@mir.wustl.edu).

Linda Larson-Prior is with the Mallinckrodt Institute of Radiology and Department of Neurology, Washington University School of Medicine, St. Louis, MO 63110 USA (phone: 314-362-7318; fax: 314-362-6971; e-mail: lindap@npg.wustl.edu).

II. METHODS

With approval by our institutional review board (HRPO), we collected data from subjects undergoing invasive monitoring for intractable epilepsy (10 grids). ECoG data were collected over several days, providing multiple epochs of non-rapid eye movement sleep (NREM) and wake. Five-minute artifact-free segments representative of NREM sleep (N2 and N3/SWS) and awake states were extracted from these longer data sets by visual inspection. Ten 30-second data segments were cut from each 5-minute segment to yield 10 data sections for each state of sleep. Data were discretized using 2048 frequency samples from 0.2 Hz to 200 Hz such that their logarithms were equally spaced. The method of Welch was used to calculate the power spectral density (PSD) at these frequencies[16]. From these PSD representations, power law signatures ($1/f$ characteristics) are extracted at band limited intervals using the methods below.

The following notations are used to further facilitate description of the techniques presented:

P_n	**PSD of *n*th observation(data from a single sensor within a 30-second interval);**
P_n'	**$\log_{10}$ space PSD of *n*th observation;**
$\hat{P}_n$	**piecewise linear representation of P_n';**
f'	**frequency in $\log_{10}$ space, i.e. $\log_{10} f$;**
S	**number of adjacent linear segments used in $\hat{P}_n$;**
E_j	**unique set of segment endpoints $\{e_1 \ldots e_{S+1}\}$;**
C	**number of classes (brain states);**
N_c	**number of training observations in class *c*;**
$\boldsymbol{z}_{cn}$	***S*-dimensional feature vector for representing the *n*th observation in class *c*;**
$\boldsymbol{Z}_c$	***S*xN_c feature matrix composed of N_c feature vectors.**

Scale-free behavior is modeled using the line slopes of a piecewise linear approximation of captured signal power for each subject and brain state. Each subject is represented by data collected from a single ECoG grid consisting of L sensors (typically between 20 and 64) and $T=10$ time intervals, where each time interval is 30 seconds long. This results in ($LxT = N$) observations of brain state for each subject and sleep stage. For each observation, the piecewise linear approximation can be written as:

$$\log P_n(f') = P_n' \approx \hat{P}_n \qquad \textbf{(1)}$$

$$= \begin{cases} \alpha_1 f' + b_1 & \text{where } e_1 \le f' < e_2 \\ \alpha_2 f' + b_2 & \textit{where } e_2 \le f' < e_3 \\ \vdots & \\ \alpha_S f' + b_S & \text{where } e_S \le f' \le e_{S+1} \end{cases}$$

where line segment endpoints, e_s, are selected from a set of 19 frequencies approximately equally distributed in log space along the frequency axis (0.2, $0.2\sqrt{2.5}$, 0.5, $0.5\sqrt{2}$, 1, $1\sqrt{2}$, 2, $2\sqrt{2.5}$, 5, $5\sqrt{2}$, 10, $10\sqrt{2}$, 20, $20\sqrt{2.5}$, 50, $50\sqrt{2}$, 100, $100\sqrt{2}$, and 200 Hz). Lines in these intervals are described by intercepts, b_s, and slopes, α_s. These slopes are of primary interest in our modeling of the small-world network characteristics of brain state.

While e_1 and e_{S+1} are fixed at 0.2 Hz and 200 Hz, unique partitions of the frequency band f' can be generated by varying the relative positions of intermediate segment endpoints. Each of these unique partitions is said to be represented by the endpoint set E_j and results in a unique characterization of the source signal's scale-free properties.

A. Best Fit MMLA

The task of selecting one of these unique sets of partition endpoints is addressed by our best-fit MMLA method. This technique extracts PSD power law signatures using minimum error straight line curve fits in order to observe the discriminatory potential of these features. This technique provides a mechanism to characterize scale-free properties of data without *a priori* knowledge of the source state. That is, a frequency band partitioning scheme, E_j, is selected not based on the resulting discriminatory power, but on the error of the computed linear fit.

Piecewise linear fitting was performed using an optimized strategy which selects a set of adjacent frequency ranges that minimize the line fit error across data from all sensors. This unique partition is selected from the set of all possible combinations of adjacent frequency ranges. The piecewise linear fit is not optimal for each sensor, but the partition boundaries selected result in the minimum total error across all sensors. Fit error for partitioning E_j is computed as:

$$\boldsymbol{\varepsilon_j} = \sum_{\boldsymbol{n=1}}^{\boldsymbol{N_c}} \left[\sum_{\boldsymbol{f'=0.2Hz}}^{\boldsymbol{200Hz}} \left(\boldsymbol{P_n'} - \left(\boldsymbol{\hat{P}_n} \middle| \boldsymbol{E_j} \right) \right)^2 \right]^{\frac{1}{2}} \qquad \textbf{(2)}$$

where f' takes on the discretely sampled frequencies in the log-log PSD plot. The least-error representation is determined as:

$$r_a = \arg\min_j \{\varepsilon_j\}. \qquad \textbf{(3)}$$

The highest ranked partitioning scheme, $\left(E_j \middle| MIN\{\varepsilon_j\}\right)$, is used to extract feature vectors and matrices to model the source brain state, c. Quantifying PSD data in this way requires no *a priori* knowledge of the sample's class label or assumption concerning specific frequency ranges to target.

An analysis of $\hat{P}_n$ line fit error indicates that a four-segment piecewise linear fit provides a reasonable representation of the source data, P_n'. Fig. 1 shows the relative line fit error when using $S=1..8$ piecewise linear segments to approximate P_n'. The $S=4$ segment representation strikes a balance between fitting a single non-representative line to the entire data set and over representing PSD details, which only obfuscates proposed power law signature characteristics. This analysis agrees with our initial studies [15] in that average fit error improved less than 5% by modeling PSD slopes with more than four segments.

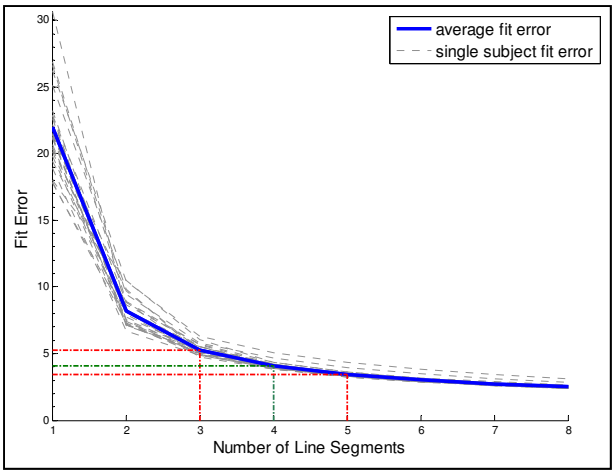

Fig. 1. Line fit error, ε_j, vs. number of line segments used to approximate P_n' with $\hat{P}_n$. Dashed grey lines indicate data from individual subjects, while the solid blue line represents the average fit error across all subjects. Green and red dashed lines highlight the decreasing change in line fit error when using three, four and five piecewise linear segments to approximate P_n'.

B. Discriminatory Value Quantification

Features extracted using this method are selected based on their ability to most accurately fit the source data's piecewise linear estimation. Of course, there is no guarantee that this same modeling scheme will provide feature measures with desirable characteristics in terms of neural state discrimination. A straightforward classification system is needed to provide a metric estimating the features' value in state discrimination. The Bayes classifier is used here to implement maximum likelihood analysis and partition class feature data.

An inspection of slope-value histograms shows normal distribution of slope values when considering a single line fit segment's characteristic across channels and time intervals. For this reason, a Gaussian mixture model was selected to represent class characteristics in feature space, $\boldsymbol{Z}_c$. These Gaussian distributions can be fully specified as a mean vector, $\mu_{\boldsymbol{c}}$, and covariance matrix, $\boldsymbol{\Sigma_c}$ for each class category c. It is straightforward to estimate these parameters from training data as:

$$\mu_{\boldsymbol{c}} = \frac{1}{N_c}\sum_{i=1}^{N_c} \boldsymbol{z}_{ci} \quad c = 1, 2, \ldots C \quad \textbf{and}$$
$$\boldsymbol{\Sigma_c} = \frac{1}{N_c}\sum_{i=1}^{N_c}[(\boldsymbol{z}_{ci} - \mu_{\boldsymbol{c}})(\boldsymbol{z}_{ci} - \mu_{\boldsymbol{c}})^{\mathrm{T}}] \tag{4}$$

for each class $c = 1..C$, where $\boldsymbol{z}_{ci}$ represents a single observation of slope of class c and N_c is the total number of observations included in the training set for that class. It follows from the definition of the Bayes classifier with a Gaussian mixture model that a discriminant function can be computed as

$$d_c(\boldsymbol{z}) = P(\omega_c)\frac{1}{(2\pi)^{S/2}|\boldsymbol{\Sigma}_c|^{1/2}} e^{-\frac{1}{2}(\boldsymbol{z}-\mu_c)^{\mathrm{T}}\boldsymbol{\Sigma}_c^{-1}(\boldsymbol{z}-\mu_c)} \quad \boldsymbol{c} = 1, 2, \ldots C \tag{5}$$

where $P(\omega_c)$ is the *a priori* probability of feature vector $\boldsymbol{z}$ belonging to class c (the prior probabilities of each class are assumed to be equal). The remainder of the equation is simply derived from the scaled and shifted expression of the multivariate normal density $N(\boldsymbol{\mu_c}, \boldsymbol{\Sigma_c})$. When presented with a new observation, category assignment is determined by selecting class i for which $d_i(\boldsymbol{z}) > d_j(\boldsymbol{z})$ for all $i \neq j$.

The effectiveness of the MMLA data-driven approach to feature extraction was quantified using an intra-subject train-test approach. The feature matrix $\boldsymbol{Z}_c$ is extracted for each set of $\hat{P}_n$ and E_j where E_j is ranked as r_a. These class specific feature matrices, $\boldsymbol{Z}_{c=1,..,C}$, are used to compute discriminant functions. Finally, the classification accuracy of the frequency band partitioning scheme, $CA(\boldsymbol{Z}_{c=1,..,C}|E_j)$, is calculated as the ratio of correctly classified observations vs. total number of observations.

C. Benchmark Development

It is difficult to establish the relative value of a feature extraction method without some frame of reference. Our benchmark model measures classifier performance using slope features extracted from all possible partitioning, E_j for all j, of PSD data. By examining all representations of PSD slope, we seek to estimate availability of discriminatory information contained within these band limited power law signatures, determined by $\alpha_{k,}\ k = 1,..,S$ in Eq. (1). *A posteriori* knowledge of sample state is used to determine some best frequency band partitioning, E_j, resulting in minimum-error state discrimination. This method does not preselect a frequency partitioning as in the best-fit MMLA approach; rather it searches all possible full band partitions and highlights the most discriminative representation. This establishes some useful limits of the technique.

For each observation of a brain state a model is constructed as the feature vector $\boldsymbol{z}_{cn}$. This S element vector is composed of the line slopes $\alpha_1 \ldots \alpha_S$. The state of class c (where c is SWS, N2 or Awake) is modeled by the SxN_c feature matrix $\boldsymbol{Z}_c$, where each of N_c columns is a unique feature vector, $\boldsymbol{z}_{cn}$. Let $CA(\boldsymbol{Z}_{c=1,..,C}|E_j)$ be the classification accuracy of model $\boldsymbol{Z}_{c=1,..,C}$ given partitioning E_j. The unique endpoint set which results in the highest classification accuracy can then determined by:

$$r_b = \arg\max_j\{CA(\boldsymbol{Z}_{c=1,..,C}|E_j)\} \tag{6}$$

where r_b is the classification accuracy related to the frequency band partitioning, E_j, and the most discriminatory representation of the source PSD's scale-free properties.

With the determination that an $S=4$ segment fit is appropriate, we show an example of the two PSD partitioning schemes in Fig. 2. The best-fit MMLA approach selects E_j for which minimum line fit error is achieved across all P_n' (Fig 2 top). A similar, but unique, full band partitioning scheme, which results in maximum classification accuracy, r_b, is selected as the *benchmark* (Fig 2 bottom). The differences between these representations of

the source PSD is of interest in determining the value of a best-fit MMLA feature selection method.

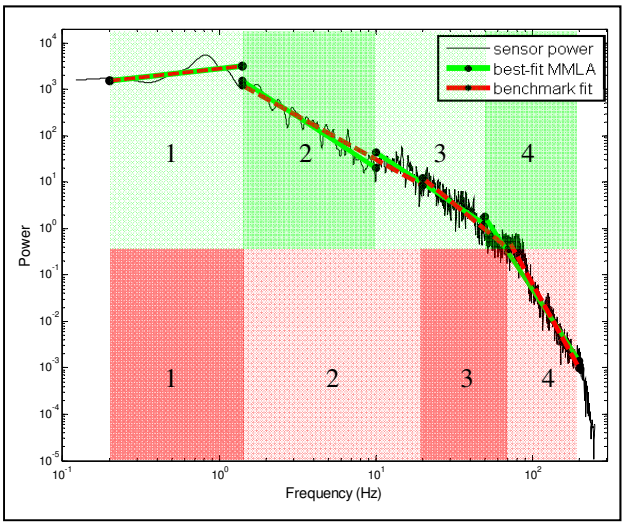

Fig. 2. Two unique frequency band partitions of a single sensor PSD determined by best-fit MMLA (top green) and maximum classification accuracy benchmark (bottom red). Best-fit MMLA partition endpoints are selected to minimize the error between a four-segment piecewise linear model and the source PSD. Benchmark endpoints are selected to maximize classifier accuracy based on the slopes of the resultant line segments.

III. RESULTS

Analysis was performed using data from 2 class categories (SWS, Awake) for all subjects and 3 class categories (SWS, Awake, N2) for Subjects 1-6. Based on the characteristics shown in Fig. 2, S=4 adjacent line segments were used to approximate PSD data and $1/f$ characteristics. While it is necessary to select S=4 based purely on unlabeled source data to be useful in a state classifier, benchmark analysis affords the opportunity to explore the relative value of this selection. Fig. 3 shows the classification accuracy, $CA\left(\boldsymbol{Z}_{c=1,..,C}\middle|E_j\right)$, achieved where j results in r_b for S=1,..,8. That is, maximum classification accuracy achieved with an S segment linear fit of source PSDs.

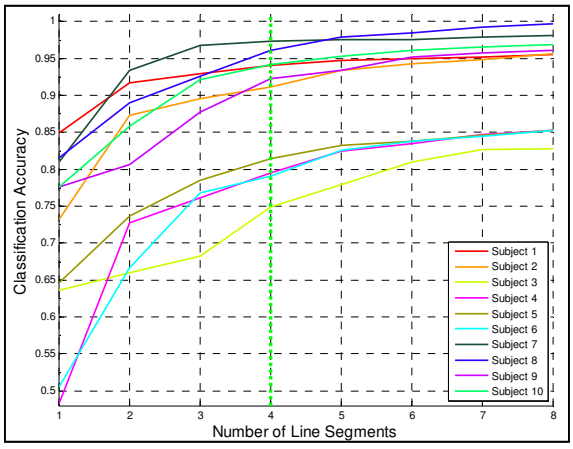

Fig. 3. Classification accuracy vs. number of line segments used to approximate P_n' with $\hat{P}_n$. Each line indicates the maximum classification accuracy achieved using benchmark analysis to select segment endpoints, E_j. The vertical green line denotes S=4, as implemented in this work.

For most subjects, classification accuracy using S=4 is within 5% of the maximum; where the curves become nearly flat. These responses support the conclusion drawn from Fig. 1 that a four segment approximation is a reasonable choice for representing P_n' for the purposes of state discrimination.

While Fig. 3 demonstrates that using curve fit error to determine the number of segments to form the piecewise representation of P_n', our primary goal in establishing a benchmark is to evaluate the performance of our best-fit MMLA approach. Fig. 4 shows the relationship between line segment fit error and the resultant classification accuracy as computed in our benchmark analysis. Each data point corresponds to $CA\left(\boldsymbol{Z}_{c=1,..,C}\middle|E_j\right)$ and the associated ε_j, computed using Eq. (6), for every endpoint set, E_j. Results shown are computed using data from Subject 1, where classes include SWS, N2 and Awake.

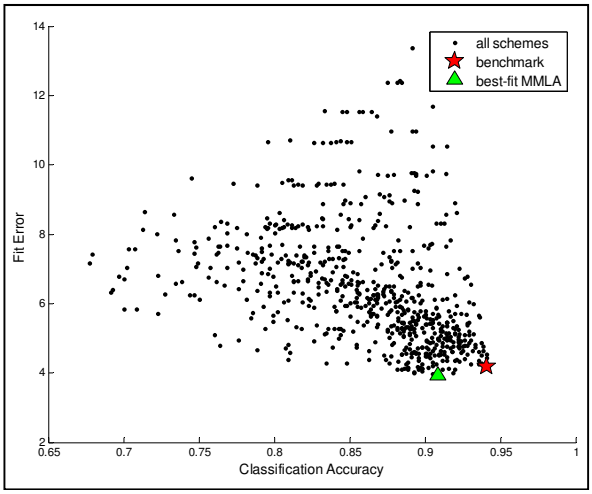

Fig. 4. Performance characteristics of S=4 partitioning scheme. Plot shows E_j, $CA\left(E_j\right)$ pairs for Subject 1 in black. Distribution of plot points demonstrates a positive relationship between low line-fit error and high classification accuracy. The maximum classification accuracy found using benchmark analysis is shown as a red star. The classification accuracy resulting from best-fit MMLA is shown as a green triangle. Note the proximity of both points toward minimum fit error achieved with the four segment linear fit.

It is clear from the distribution of benchmark operating points, ε_j vs. $CA\left(\boldsymbol{Z}_{c=1,..,C}\middle|E_j\right)$, that a trend between low fit error and high classification accuracy exists. This distribution is typical across all subject data studied for both the 2 and 3-class cases. The best performing operating point is indicated in red, with 94.06% classification accuracy. The resultant performance reported by best-fit MMLA is shown in green, with 90.83% classification accuracy. In this case the performance of our power law representation nearly matches that of the *a posteriori* based benchmark. Both frequency partitions result in low fit error and high accuracy, however, the improved performance realized using the optimized benchmark may be an indication that there are additional characteristics of the source PSD that could be used to fine-tune techniques used our approach.

Table 1. Comparing classifier performance of best performing benchmark (BM) technique and of that of the best-fit MMLA method. Discriminating SWS from awake (A), SWS, N2, awake (B).

	A (SWS and awake)			B (SWS, N2, awake)		
Subject	BM (%)	MMLA (%)	% diff	BM (%)	MMLA (%)	% diff
1	100	99.22	0.78%	94.06	90.83	3.23%
2	100	100	0.00%	91.17	86.17	5.00%
3	89.76	87.86	1.90%	74.87	72.7	2.17%
4	97.79	94.74	3.05%	79.53	71.41	8.12%
5	98.47	90.15	8.32%	81.42	68.63	12.79%
6	96.8	97.03	0.23%	79.06	77.19	1.87%
7	97.34	80.55	16.79%			
8	96.05	90.53	5.52%			
9	92.26	79.84	12.42%			
10	94.21	75	19.21%			

Table 1 A and B detail the performance variations between our best-fit MMLA and the highest ranked benchmark for all subjects in the studied population. Table 1A illustrates performance when attempting to discriminate between slow wave sleep (SWS) and Awake brain states. Benchmark classification is high across all subjects, indicating that the global 1/*f* characteristics contain information which supports discrimination between these two brain states. It should be noted that discriminability, while generally high, does vary by subject. This may be relevant to pathological populations and warrants further investigation.

Table 1B shows 3-class system performance for Subject 1 through Subject 6 (all subjects for which SWS, N2 and Awake data were available). Results from the BM column show that reasonable discriminatory power exists within the measured characteristics. Techniques implemented in MMLA demonstrate similar performance results, with a few exceptions noted below

The performance variation between techniques is seen for Subject 10. An inspection of the ε_j vs. $CA\left(\boldsymbol{Z}_{c=1,..,C}\middle|E_j\right)$ operating points, as in Fig. 4, shows that many near-minimum-error endpoint schemes exist which produce greater than 90% classification accuracy. The circumstances are similar for other large performance disparities (Subjects 4, 5, 7, and 9). While MMLA based classification accuracies for these data are reasonable, this inspection further highlights the potential benefit available from combining best-fit 1/*f* features with other measured characteristics in an effort to improve classifier performance.

IV. Conclusion

We have shown that global properties represented in 1/*f* scaling in human ECoG contain sufficient information to discriminate substates of NREM sleep. We further show that, using a four-segment piecewise linear fit provides a reasonable representation of the source data and can be accomplished without prior knowledge of the state represented. Finally, we show that where fit error is low, state classification accuracy is high. While this supports the validity of our feature extraction approach, we see variability in the ability to discriminate state. This suggests that optimization of our technique requires additional features be included in the classifier to improve accuracy and reliability. Future studies will examine the utility of additional temporal characteristics of state transitions in the feature space of the classifier. Model validation will be performed using non-segmented data sets where state is not known prior to classification.

References

[1] H.-J. Park, J.-S. Oh, D.-U. Jeong et al., "Automated Sleep Stage Scoring Using Hybrid Rule- and Case-Based Reasoning," Computers and Biomedical Research, vol. 33, no. 5, pp. 330-349, 2000.

[2] S. Kubicki, and W. M. Herrmann, "The Future of Computer-Assisted Investigation of the Polysomnogram: Sleep Microstructure," Journal of Clinical Neurophysiology, vol. 13, no. 4, pp. 285-294, 1996.

[3] M. Villa, S. Piro, A. Dotta et al., "Validation of automated sleep analysis in normal children," European Respiratory Journal, vol. 11, no. 2, pp. 458-461, 1998.

[4] J. Caffarel, G. Gibson, J. Harrison et al., "Comparison of manual sleep staging with automated neural network-based analysis in clinical practice," Medical and Biological Engineering and Computing, vol. 44, no. 1, pp. 105-110, 2006.

[5] A. Picot, H. Whitmore, and F. Chapotot, "Automated detection of sleep EEG slow waves based on matching pursuit using a restricted dictionary." pp. 4824-4827.

[6] B. Kemp, "Measurement of sleep," Prog Brain Res, vol. 185, pp. 21-35, 2010.

[7] Y. Nir, R. J. Staba, T. Andrillon et al., "Regional slow waves and spindles in human sleep," Neuron, vol. 70, no. 1, pp. 153-69, Apr 14, 2011.

[8] T. Andrillon, Y. Nir, R. J. Staba et al., "Sleep Spindles in Humans: Insights from Intracranial EEG and Unit Recordings," The Journal of Neuroscience, vol. 31, no. 49, pp. 17821-17834, 2011.

[9] C. Bedard, H. Kroger, and A. Destexhe, "Does the 1/f Frequency Scaling of Brain Signals Reflect Self-Organized Critical States?," Physical Review Letters, vol. 97, no. 11, pp. 118102, 2006.

[10] W. J. Freeman, M. D. Holmes, G. A. West et al., "Fine spatiotemporal structure of phase in human intracranial EEG," Clinical neurophysiology : official journal of the International Federation of Clinical Neurophysiology, vol. 117, no. 6, pp. 1228-43, Jun, 2006.

[11] B. J. He, A. Z. Snyder, J. M. Zempel et al., "Electrophysiological correlates of the brain's intrinsic large-scale functional architecture," Proceedings of the National Academy of Sciences of the United States of America, vol. 105, no. 41, pp. 16039-44, Oct 14, 2008.

[12] J. Chu-Shore, M. B. Westover, and M. T. Bianchi, "Power Law versus Exponential State Transition Dynamics: Application to Sleep-Wake Architecture," PLoS One, vol. 5, no. 12, pp. e14204, 2010.

[13] W. Freeman, and J. Zhai, "Simulated power spectral density (PSD) of background electrocorticogram (ECoG)," Cognitive Neurodynamics, vol. 3, no. 1, pp. 97-103, 2009.

[14] B. J. He, J. M. Zempel, A. Z. Snyder et al., "The temporal structures and functional significance of scale-free brain activity," Neuron, vol. 66, no. 3, pp. 353-69, May 13, 2010.

[15] J. M. Zempel, D. G. Politte, M. Kelsey, R. Vernier, T. S. Nolan, A. Babajani-Feremi, F. Prior, L. J. Larson-Prior, "Characterization of scale-free properties of human electrocorticography in awake and slow wave sleep states," Frontiers in Sleep and Chronobiology, in press, 2012.

[16] P. Welch, "The use of fast Fourier transform for the estimation of power spectra: A method based on time averaging over short, modified periodograms," Audio and Electroacoustics, IEEE Transactions on, vol. 15, no. 2, pp. 70-73, 1967.